Mathematical and Computer Modelling 54 (2011) 2493–2503

Contents lists available at ScienceDirect

Mathematical and Computer Modelling

journal homepage: www.elsevier.com/locate/mcm

Stability of delay integro-differential equations using a spectral element method

Firas A. Khasawneh *, Brian P. Mann

Mechanical Engineering and Materials Science Department, Duke University, Durham, NC 27708, United States

ARTICLE INFO

Article history:
Received 23 November 2010
Received in revised form 22 May 2011
Accepted 5 June 2011

Keywords:
Delay equations
Delay integro-differential equations
Spectral element
Stability

ABSTRACT

This paper describes a spectral element approach for studying the stability of delay integro-differential equations (DIDEs). In contrast to delay differential equations (DDEs) with discrete delays that act point-wise, the delays in DIDEs are distributed over a period of time through an integral term. Although both types of delays lead to an infinite dimensional state-space, the analysis of DDEs with distributed delays is far more involved. Nevertheless, the approach that we describe here is applicable to both autonomous and non-autonomous DIDEs with smooth bounded kernel functions. We also describe the stability analysis of DIDEs with special kernels (gamma-type kernel functions) via converting the DIDE into a higher order DDE with only discrete delays. This case of DIDEs is of practical importance, e.g., in modeling wheel shimmy phenomenon. A set of case studies are then provided to show the effectiveness of the proposed approach.

The evolution of the states in a system are often governed not only by the current states, but also by the past ones. These systems are described mathematically by delay differential equations (DDEs) where the delay leads to infinite dimensional state-space. When the delay is a discrete scalar that acts at a single instant of time it is called a concentrated or discrete delay. However, in many applications the effect of the delay is distributed over a time interval according to the delay integro-differential equation (DIDE)

$$\dot{x}(t) = f\left(x(t), \int_0^{\vartheta} K(t,s)x(t-s)\mathrm{d}s\right), \tag{1a}$$

$$x(t) = \varphi(t) \quad \text{for } t \in [-\vartheta, 0], \tag{1b}$$

where $x \in \mathbb{R}^n, f : \mathbb{R}^n \times \mathbb{R}^n \to \mathbb{R}^n$ is continuously differentiable, φ is continuous and it represents the history segment, $K : \mathbb{R} \times \mathbb{R} \to \mathbb{R}^{n\times n}$ is a bounded analytic kernel function while $\vartheta > 0$ is the duration of the bounded distributed delay. Examples where several variations of Eq. (1) appear include wheel shimmy models [1–3], traffic models [4–8], machining dynamics [9,10], and neural modeling [11]. A common interest in all these application areas is the stability of equilibria in the governing DIDE. More specifically, in this study we are interested in the stability of Eq. (1) where f is linear in both $x(t)$ and $x(t-s)$.

The stability analysis of DIDEs is more complicated than delay differential equations (DDEs) with discrete delays due to the added complexity of the integral term. This is evidenced by the limited number of studies on DIDEs compared to the more extensive literature on DDEs with discrete delays. Nevertheless, several methods have been used in literature for studying DIDEs.

For instance, the stability conditions of Runge–Kutta type methods for DIDEs were investigated in Refs. [12,13]. Baker and Ford studied the stability of scalar DIDEs with a constant kernel using numerical schemes based on the Newton–Cotes formula combined with a linear multi-step method [14].

* Corresponding author. Tel.: +1 919 660 5338; fax: +1 919 660 8963.
E-mail addresses: firas.khasawneh@duke.edu (F.A. Khasawneh), bpm4@duke.edu (B.P. Mann).

0895-7177/$ – see front matter © 2011 Elsevier Ltd. All rights reserved.
doi:10.1016/j.mcm.2011.06.009

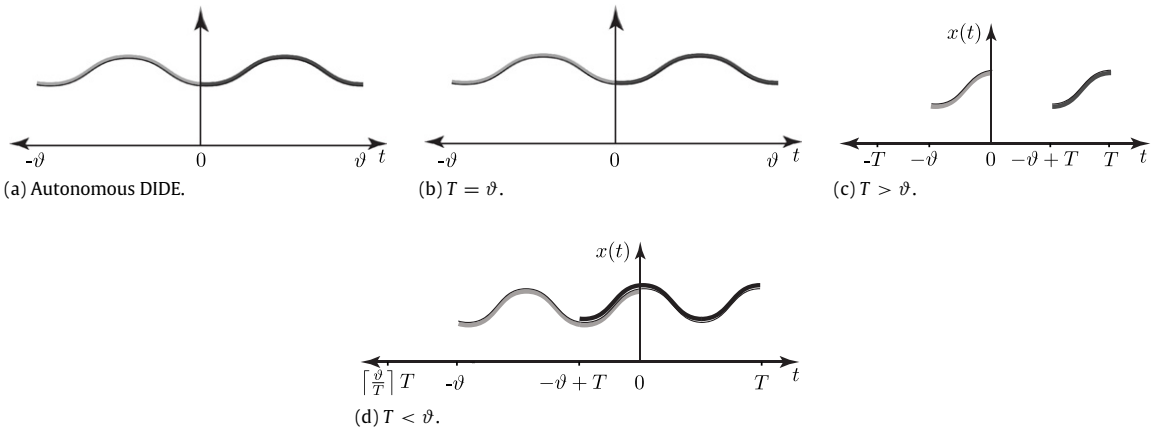

(a) Autonomous DIDE. (b) $T = \vartheta$. (c) $T > \vartheta$. (d) $T < \vartheta$.

Fig. 1. An example mapping of the system states (light gray line) one period ahead (dark gray line) for (a) autonomous as well as (b)–(d) time-periodic DIDEs.

Luzyanina and Roose used a linear multi-step method and a Gauss quadrature to find the stability of scalar DIDEs [15]. Both constant and non-constant kernels comprised of trigonometric and polynomial functions were investigated. Further, computational techniques for discrete DDEs were applied to DIDEs with special kernels in Ref. [16]. Specifically, the kernel functions were either constant or had a gamma-type distribution.

Kiss and Krauskopf studied the stability of DIDEs with symmetric kernel functions by considering a corresponding DDE where the delay was fixed and was given by the mean of the kernel [17,18]. However, the analysis of Kiss and Krauskopf is only valid for autonomous DIDEs with symmetric kernel functions and cannot be used for non-autonomous DIDEs or DIDEs with asymmetric kernel. Further, the applicability of their results is limited to scalar DIDEs or second order DIDEs with non-instantaneous feedback, i.e., second order DIDEs where the dependent variable only appears in delayed form.

Insperger and Stepan used the semi-discretization method to study the stability of DIDEs for various constant and non-constant kernels [19]. The semi-discretization method divides the time-line into short intervals on which an approximate analytical solution can be obtained. The collection of these expressions can then be used to create a finite dimensional transition matrix which approximates the infinite dimensional monodromy operator of the DDE. A higher order version of the semi-discretization method was also presented in Ref. [20]. However, the semi-discretization method can result in large matrices to produce a convergent solution.

Breda et al. presented an approach to ascertain the stability of DIDEs using the discretization of the infinitesimal generator of the solution operators semigroup [21]. The approximate eigenvalues were then found by solving a large sparse standard eigenvalue problem. However, this approach has been only used for autonomous DIDEs. Further, the size of the resulting matrices can in some cases cause computational difficulties.

The above survey on methods for solving DIDEs revealed that the related research has mostly been focused on stability of numerical schemes for DIDEs with special types of kernel (mostly symmetric, constant or gamma-type) or DIDEs with autonomous coefficients. Therefore, in this paper we describe a spectral element approach for the stability analysis of delay equations with distributed delays. Specifically, both autonomous and non-autonomous DIDEs will be investigated for general bounded and smooth kernel functions.

This paper is organized as follows. Section 1 describes the extension of the spectral element approach to DIDEs. Section 2 provides the stability diagrams of some case studies including both autonomous and time-periodic DIDEs. Section 3 studies a special case of DIDEs that can be reduced to a DDE with only discrete delay. The paper ends with conclusions in Section 4.

1. Stability analysis of DIDE using spectral element

This section describes a spectral element approach for the stability analysis of DIDEs. This approach has recently been developed for DDEs with discrete delays and was proven to have faster rates of convergence than the collocation and the temporal finite element methods [22].

The spectral element method is a Galerkin-type technique that discretizes the state space and creates a dynamic map between the history segment and the evolved states one period ahead (see Fig. 1). The matrix describing the map is called the monodromy matrix and it represents a finite dimensional approximation to the infinite dimensional monodromy operator. The stability of the system is then determined by the eigenvalues of the monodromy matrix. The spectral element approach offers substantial improvements over the authors' prior works on the temporal finite element approach (TFEA). To elaborate, the spectral element method discretizes the state space using a more accurate and more numerically stable interpolation formula on a well-conditioned set of mesh points. The weighted residual integral is approximated using a highly accurate Gauss quadrature instead of the tedious and time consuming (and sometimes unfeasible) symbolic integrals. The spectral element approach is therefore superior to the temporal finite element approach(TFEA) in every aspect and it yields higher

rates of convergence than TFEA and allows *hp*-convergence schemes where both the number of elements and the order of the interpolating polynomial can be increased to obtain convergence. Ref. [22] provides a more thorough comparison between the spectral element approach and TFEA. We will describe the spectral element approach in more detail in the following sections but we list here the basic steps of the analysis:

1. Discretizing the integral term in the DIDE.
2. Discretizing the state space.
3. Constructing the monodromy matrix.

These steps are described in more detail in the following sections. Specifically, Section 1.1 describes the discretization of the integral term in the DIDE using a Gauss quadrature rule. Section 1.2 describes a polynomial approximation scheme based on Lagrange interpolation for discretizing the state space of the DIDE. Section 1.3 then uses the method of weighted residuals to reduce the error associated with approximating the states and to construct a dynamic map over one period. The matrix describing the map is called the monodromy matrix and its eigenvalues are used to ascertain the stability of Eq. (1).

1.1. Discretizing the integral

The first step in the analysis that follows is to discretize the integral term in the DIDE using a suitable quadrature rule. Specifically, an mth order Gauss quadrature rule can be used to approximate integrals according to

$$\int_a^b f(t)\,\mathrm{d}t \approx \frac{b-a}{2}\sum_{k=1}^{m+1} w_k^* f(t_k), \tag{2}$$

where t_k and w_k^* are the Gauss quadrature nodes and weights, respectively. In this study we use the Legendre–Gauss–Lobatto points (LGL) obtained from solving for the roots of the equation

$$(1-u^2)L_m'(u) = 0, \tag{3}$$

where u ranges from -1 to 1 and $L_m(u)$ is the Legendre polynomial of order m [23]. The corresponding quadrature weights are obtained using

$$w_k^* = \begin{cases} \dfrac{2}{m(m+1)} & k = 1, m+1 \\ \dfrac{2}{m(m+1)(L_m(\eta_k))^2}, & \text{otherwise.} \end{cases} \tag{4}$$

The LGL points can be shifted to an arbitrary interval $[a, b]$ through the relation

$$\tilde{u} = \frac{b-a}{2}u + \frac{b+a}{2}, \tag{5}$$

where $u \in [-1, 1]$ and $\tilde{u} \in [a, b]$, e.g., $a = 0$ and $b = \vartheta$ in Eq. (1).

Eq. (2) yields accurate results for integrands that can be approximated by polynomials of order $2m+1$ [15]. Throughout this paper we will assume that the integrand is well approximated by such a polynomial and fix the number of the quadrature points to $m+1$.

Using Eq. (2) to approximate the distributed delay integral in Eq. (1) gives

$$\dot{x}(t) - f\left(x(t), \frac{\vartheta}{2}\sum_{k=1}^{m+1} w_k^* K(t, s_k)x(t-s_k)\right) = 0. \tag{6}$$

1.2. Discretizing the state space

The next step is to divide the interval $[0, T]$ into E temporal elements as shown in Fig. 2(a). If the system is autonomous, then the choice $T = \vartheta$ is made to simplify the analysis. Consider for example the jth element defined on the interval

$$e_j = [t_j^-, t_j^+), \tag{7}$$

where t_j^- and t_j^+ are the left and right endpoints of the jth element, respectively, while h_j is the length of the jth element and is given by

$$h_j = t_j^+ - t_j^-. \tag{8}$$

A set of $n+1$ interpolation nodes is then defined within each element as shown in Fig. 2(b). Any set of distinct $n+1$ points can be used; however, the numerical stability of the approximation is improved if the roots or extrema of orthogonal functions

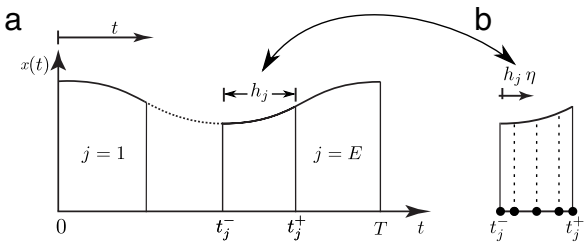

Fig. 2. Discretization of the state space into temporal elements (Fig. (a)) and the interpolation nodes within each element (Fig. (b)).

is used. Therefore, in this study we will use the LGL points derived from Eqs. (3) and (5) as the interpolation nodes. These nodes are used to define a local approximate expression for the states within each element according to

$$x_j(t) = \sum_{i=1}^{n+1} x_{ji}\phi_i(\eta), \tag{9}$$

where $\eta \in [0, 1]$ is the local time normalized by the length of the element h_j while the trial function $\phi_i(\eta)$ can be obtained using the Lagrange formula; however, the typical form of Lagrange interpolation is only recommended for a small number of nodes to avoid numerical instabilities associated with higher order interpolants [24]. A more effective representation of Lagrange polynomials is provided by the barycentric formula according to

$$\phi_i(\eta) = \frac{\frac{\varpi_i}{\eta-\eta_i}}{\sum_{k=1}^{n+1}\frac{\varpi_k}{\eta-\eta_k}}, \tag{10}$$

where η_i and η_k are the ith and kth interpolation nodes, respectively, while ϖ_k are the barycentric weights given by

$$\varpi_k = \frac{1}{\prod_{k\neq j}(\eta_j - \eta_k)}, \quad j = 1, \ldots, n+1. \tag{11}$$

The barycentric formula has better numerical stability than the conventional Lagrange representation [24,25]; therefore, it was used to generate the trial functions in the present study.

In addition to being a more efficient tool to generate the trial functions, the barycentric weights can be used to obtain the value of the derivative of the trial functions evaluated at the interpolation nodes according to

$$\phi_i'(\eta_k) = \begin{cases} \dfrac{\varpi_i/\varpi_k}{\eta_i - \eta_k}, & i \neq k \\ \displaystyle\sum_{i=0, i\neq k}^{n+1} \frac{-\varpi_i/\varpi_k}{\eta_i - \eta_k}, & i = k. \end{cases} \tag{12}$$

The values defined in Eq. (12) form the entries of the differentiation matrix which describes a linear transformation from the values of the trial functions at the nodes to the values of the derivative of the trial functions at the same nodes. For example, assume that the vector $\mathbf{z}$ contains the values of a function $g(t)$ evaluated at the $n+1$ LGL points. If the vector $\mathbf{z}'$ contains the derivative of g evaluated at the same collocation points, then the effect of differentiating the function at these points can be described by a differentiation matrix $\mathbf{D}$ according to

$$\mathbf{z}' = \mathbf{D}\,\mathbf{z}, \tag{13}$$

where the entries of $\mathbf{D}$ are defined from Eq. (12) according to

$$D_{ki} = \phi_i'(\eta_k). \tag{14}$$

Using the LGL nodes simplifies the expression for the $(n+1) \times (n+1)$ differentiation matrix in Eq. (13) to

$$D_{00} = -D_{nn} = -\frac{n(n+1)}{4}, \tag{15a}$$

$$D_{km} = \begin{cases} \dfrac{L_n(t_k)}{L_n(t_m)}\dfrac{1}{(t_k - t_m)}, & k \neq m \\ 0, & \text{otherwise.} \end{cases} \tag{15b}$$

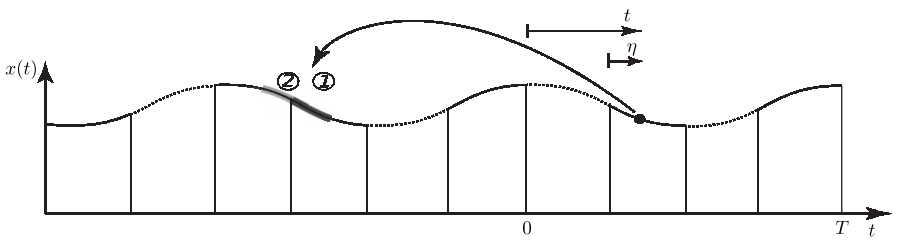

Fig. 3. The effect of the distributed delay on the mapping of the system states at time t (black dot). Each point is mapped onto an interval that can span more than one element. In this illustration, the mapping spans the two elements marked by ①and ②.

1.3. The monodromy matrix

Substituting the approximate solution over the jth element into Eq. (6) yields

$$\sum_{i=1}^{n+1} \frac{1}{h_j}\dot{\phi}_i(\eta)x_{ji} - f\left(\sum_{i=1}^{n+1}\phi_i(\eta)x_{ji},\ \frac{\vartheta}{2}\sum_{k=1}^{m+1} w_k^* K(t_j^- + \eta h_j, s_k)\sum_{i=1}^{n+1}\phi_i(\eta_k^*)x_{j^*(t_k^*),i}^{q_k}\right) = \text{error}, \tag{16}$$

where the residual error is due to the approximation procedure. The time t_k^* is defined using modular arithmetics according to

$$t_k^* = t_j^- + \eta h_j - s_k (\text{mod } T). \tag{17}$$

Eq. (17) is used to define the local normalized time according to

$$\eta_k^* = \frac{t_k^* - t_j^{*-}}{h_j^*}, \tag{18}$$

where t_j^{*-} is the left boundary of the element $j^* = j^*(t_k^*)$ while h_j^* is its length. the function $j^*(t_k^*)$ gives the element index to which t_k^* belongs and it is given by

$$j^*(t_k^*) = \sum_{j=1}^{E} j\chi_{e_j}(t_k^*), \tag{19}$$

where the indicator function is defined as

$$\chi_{e_j}(t_k^*) = \begin{cases} 1 & \text{if } t_k^* \in e_j, \\ 0 & \text{otherwise.} \end{cases} \tag{20}$$

If the elements are uniformly distributed, then Eq. (19) reduces to

$$j^*(t_k^*) = \left\lceil \frac{t_k^*}{h} \right\rceil \tag{21}$$

where $\lceil\cdot\rceil$ is the ceiling function and h is the length of each of the uniform elements.

The integer q_k in Eq. (16) is the number of periods the delay looks back and it is described by

$$q_k = \left|\left| \left\lfloor \frac{t - s_k}{T} \right\rfloor \right|\right|, \tag{22}$$

where $\lfloor\cdot\rfloor$ is the floor function and with the understanding that $q_k = 0$ indicates a mapping onto the interval $[0, T]$.

Note that for DIDEs each discretization point η_i is mapped back onto $m + 1$ points due to the integral. This mapping of a point into an interval is described in Fig. 3 where it is shown that a point can further get mapped onto more than one element. If any of the mapped points does not coincide with the discretization nodes, the interpolation described by Eq. (9) is used to obtain an expression for the mapped states in terms of the states at the $n + 1$ local nodes within the element j^*.

The method of weighted residuals is used to reduce the error in Eq. (16). Specifically, we multiply Eq. (16) with a set of linearly independent weight functions $\{\psi_p(\eta)\}_{p=1}^n$ and integrate over the length of each element according to

$$\int_0^1 \left(\sum_{i=1}^{n+1} \frac{1}{h_j}\dot{\phi}_i(\eta)x_{ji} - f\left(\sum_{i=1}^{n+1}\phi_i(\eta)x_{ji},\ \frac{\vartheta}{2}\sum_{k=1}^{m+1} w_k^* K(t_j^- + \eta h_j, s_k)\sum_{i=1}^{n+1}\phi_i(\eta_k^*)x_{j^*(t_k^*),i}^{q_k}\right)\right)\psi_p(\eta)\mathrm{d}\eta = 0. \tag{23}$$

Although Eq. (23) is linear in x, the integral can often cause computational difficulties. To elaborate, performing the above integral analytically is not always possible especially if the DIDE has complicated time-periodic coefficients. Therefore, the

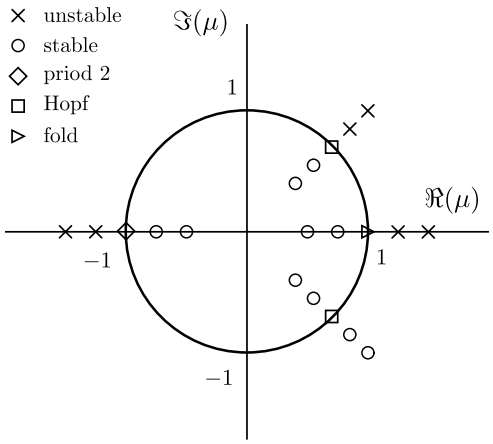

Fig. 4. The stability criteria dictates that all the eigenvalues μ of the monodromy operator U should lie within the unit circle in the complex plane. Moreover, the manner in which the eigenvalues depart the unit circle produces different bifurcation behavior as shown.

spectral element approach is made more robust by approximating the analytical integral with an accurate quadrature rule similar to Eq. (2). Using $N+1$ quadrature points and weights to approximate the integral in Eq. (23) gives

$$\sum_{r=1}^{N+1} w_r \left(\sum_{i=1}^{n+1} \frac{1}{h_j} \dot{\phi}_i(\eta_r) \psi_p(\eta_r) x_{ji} \right) - \sum_{r=1}^{N+1} w_r \left(f \left(\sum_{i=1}^{n+1} \phi_i(\eta_r) x_{ji}, \frac{\vartheta}{2} \sum_{k=1}^{m+1} w_k^* K(t_j^- + \eta_r h_j, s_k) \sum_{i=1}^{n+1} \phi_i(\eta_k^*) x_{j^*(t_k^*),i}^{q_k} \right) \psi_p(\eta_r) \right) = 0. \tag{24}$$

Recall that the Lagrange polynomial ϕ_i corresponding to the ith node has the property

$$\phi_i(\eta_k) = \begin{cases} 1, & i = k, \\ 0, & \text{otherwise}, \end{cases} \quad j, k = 1, \ldots, n+1. \tag{25}$$

Therefore, choosing the quadrature nodes to be the same as the interpolation nodes, i.e. $\{\eta_r\}_{r=1}^{N+1} = \{\eta_i\}_{i=1}^{n+1}$, in combination with Eq. (25) simplifies computing Eq. (24). Further, since f is linear in x_{ji} and $x_{j^*(t_k^*),i}^{q_k}$, applying Eq. (24) to all the elements yields a set of $n+1$ algebraic equations. Moreover, the coefficients of the states in the interval $[0, T]$ can be arranged into a matrix H while the coefficients of the states in the interval $\left[-\left\lceil \frac{\vartheta}{T} \right\rceil T, 0\right]$ can be assembled into a second matrix G. Consequently, the mapping from the states $x_{n+1} \in [0, T]$ onto $x_n \in \left[-\left\lceil \frac{\vartheta}{T} \right\rceil T, 0\right]$ is described by the dynamic map

$$x_{n+1} = U x_n. \tag{26}$$

where $U = H^{-1}G$ is the monodromy matrix which is a finite dimensional approximation to the infinite dimensional monodromy operator. The stability of Eq. (1) is then ascertained by examining the eigenvalues μ (or characteristic multipliers) of U; the system is stable if all the eigenvalues are within the unit circle in the complex plane as shown in Fig. 4.

A note on the convergence of the spectral element approach is in order. General convergence proofs for different discretizations and solution methods are very sparse in the current literature and typically focus on collocation as the solution method, e.g., [26]. In the collocation method, the evolution equation, e.g. Eq. (1), is required to hold exactly at finitely many collocation points. The spectral element method described here instead uses weighted integrals across the temporal domain. Nevertheless, there is a connection between collocation methods and the spectral element approach. Specifically, the spectral element and collocation methods differ mainly in the approach they each use to reduce the approximation error and although these two methods may seem different, they are actually closely related [27]. A discussion of the connection between the spectral element approach and collocation methods in Ref. [22] suggest that the former can be thought of as a linear transformation of the latter. Collocation methods are well documented in the literature and a proof of their convergence can be found in Ref. [26]. Since linear transformations are well behaved with respect to continuity and convergence, the spectral element approach preserves the convergence properties of the collocation approach (see Ref. [22] for more details).

2. Case studies

The effectiveness of the spectral element method for DIDEs is investigated using a set of case studies. Section 2.1 studies the stability of a scalar autonomous DIDE with a constant kernel function whereas Section 2.2 investigates a 2nd order time-periodic DIDE using various time-dependent kernel functions.

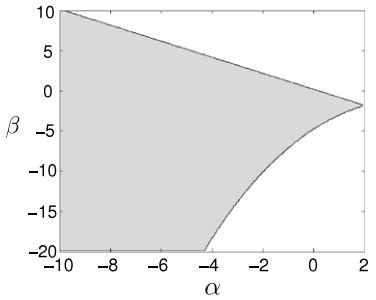

Fig. 5. The stability diagrams of Eq. (27) for different values of ϵ. The parameters used were $E = 2$, $n = 5$ and $m = 5$ while the grid size was 200×200. Stable regions are shaded while unstable regions are left unshaded.

2.1. First order DIDE

As a first example, consider the scalar DIDE

$$\dot{y}(t) = \alpha y(t) + \beta \int_0^1 y(t-s)\,\mathrm{d}s \tag{27}$$

where α and β are constants [14]. The kernel function here is constant and is equal to 1, i.e. $K(t, s) = 1$. Applying the analysis in Section 1 using $E = 2$ and $n = 5$ gives the stability diagram in Fig. 5. This diagram is in agreement with the D-subdivision results obtained in Ref. [14].

2.2. Second order DIDE with time-periodic coefficients

As a more complicated example, consider the second order time-periodic DIDE

$$\ddot{x}(t) + (\delta + \epsilon\,\cos(4\pi\,t))x(t) = \gamma \int_0^1 K(t, s)x(t-s)\mathrm{d}s, \tag{28}$$

where δ, ϵ and γ are constants while the system period is $T = 0.5$. Note that for this equation the time t appears explicitly in the function f of Eq. (1). Therefore, the spectral element approach can also handle cases where such explicit dependence on time appears in the DIDE. The stability of this equation was studied in the parameter space (δ, γ) for different values of ϵ and for various kernel functions $K(s)$. The kernel functions that were used in this study are

$$K(t, s) = \frac{\pi}{2}\sin(\pi s), \tag{29a}$$

$$K(t, s) = \frac{\pi}{2}\sin(\pi s) + \frac{13\pi}{77}\sin(2\pi s). \tag{29b}$$

The stability diagrams associated with each of these kernels are shown in Figs. 6 and 7 and they are all in agreement with the results in Ref. [19].

Fig. 6 shows the stability diagram for the kernel function in Eq. (29a). The result for the autonomous version of Eq. (28) is shown in Fig. 6 whereas the non-autonomous version is depicted in Fig. 6(b)–(d). Similar to Fig. 6, the parameters used to generate the stability diagrams in Fig. 6 are $E = 3$, $n = 10$ and $m = 15$.

Fig. 7 shows the stability diagram for the kernel function in Eq. (29b). The result for the autonomous version of Eq. (28) is shown in Fig. 7 whereas the non-autonomous version is depicted in Fig. 7(b)–(d). The parameters used to generate the stability diagrams were $E = 3$, $n = 10$ and $m = 15$.

3. Special distribution functions

For certain choices of the distribution function, namely gamma-type distributions such as exponential, gamma function and sinusoidal distributions, the integro-DDE can be transformed into a higher order DDE with only discrete delays. Hence the described techniques can be readily applied to the transformed equation to obtain stability of the original integro-DDE. Fortunately, although this choice of distribution functions is somewhat limiting, it still covers a lot of the common distributions found in physical applications [10,2].

This section uses a scalar DDE to describe the various steps of transforming an integro-DDE into a higher order DDE with only discrete delays. The same analysis was used in Ref. [10] to study the stability of a turning process at low speeds.

A first-order scalar DDE with both a discrete and a continuous delay is considered here. Using this introductory example, the procedure of transforming the equation into a form that contains only the discrete delay is described [28]. The stability of the resulting equation is then investigated using state-space TFEA.

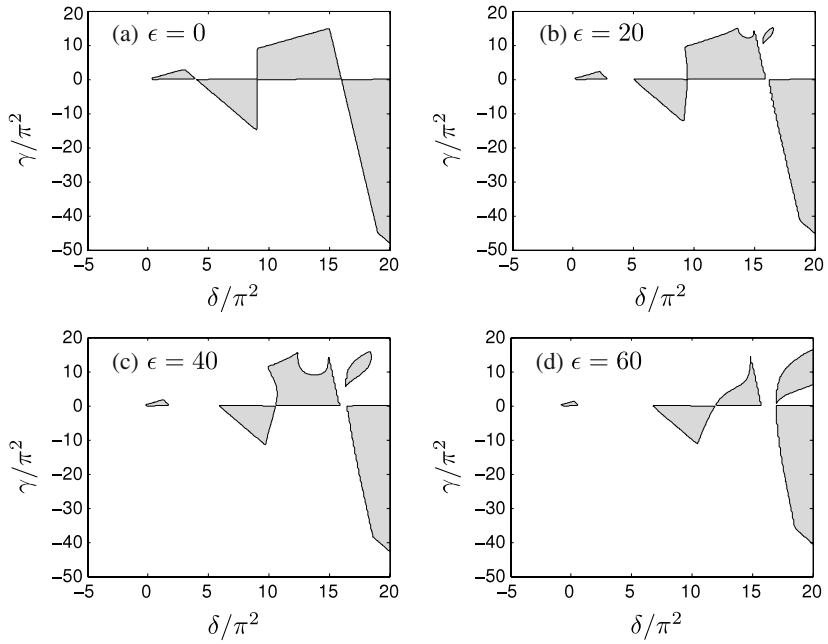

Fig. 6. The stability diagrams of Eq. (28) using the kernel function in Eq. (29a) and different values of ϵ. The parameters used were $E = 3$, $n = 10$ and $m = 15$ while the grid size was 200×200. Stable regions are shaded while unstable regions are left unshaded.

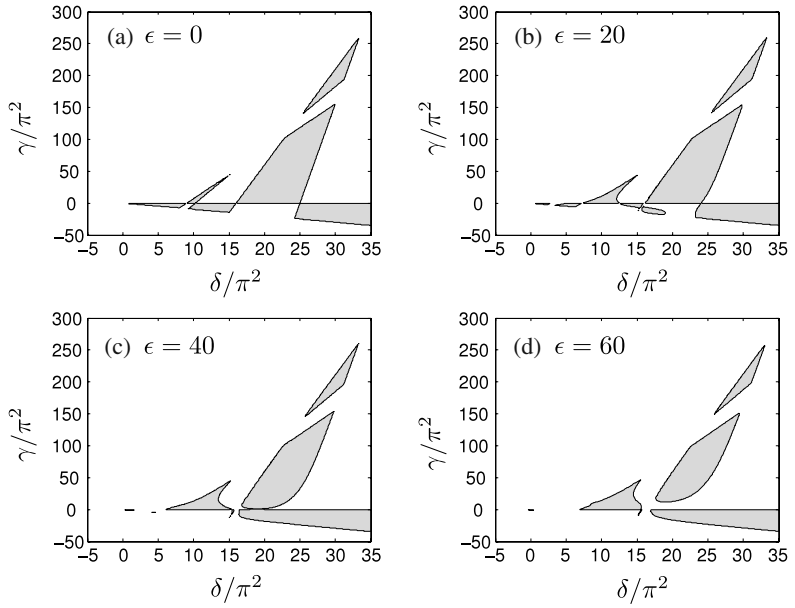

Fig. 7. The stability diagrams of Eq. (28) using the kernel function in Eq. (29b) and different values of ϵ. The parameters used were $E = 3$, $n = 10$ and $m = 15$ while the grid size was 300×300. Stable regions are shaded while unstable regions are left unshaded.

Consider the first order DDE

$$\dot{x}(t) + \alpha x(t) + \beta \int_0^{t_s} x(t - \tau - \hat{t}) w(\hat{t}) \mathrm{d}\hat{t} = 0, \tag{30}$$

where t is time, x is a real variable, α and β are real scalars, τ is a discrete delay, $\hat{t}$ is a continuous or short delay, t_s is the duration of the short delay, and $w(\hat{t})$ is a shape or weight function. To ensure convergence when the integral's upper bound is allowed to approach infinity, we require that x satisfies

$$\lim_{\hat{t} \to \infty} x(t - \tau - \hat{t}) \mathrm{e}^{\frac{-\hat{t}}{\gamma \tau}} = 0. \tag{31}$$

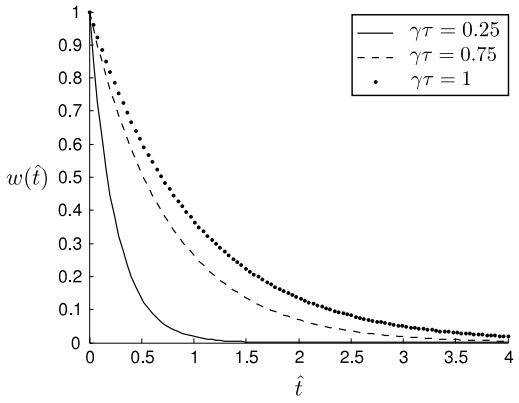

Fig. 8. The distribution function $w(\hat{t})$ in Eq. (32) using different values for $\gamma\tau$.

The integral in Eq. (30), as well as the existence of two types of delays, complicates the stability analysis of Eq. (30) in its current form. However, with a suitable choice of the weight function $w(\hat{t})$, Eq. (30) can be transformed into a solvable form. In fact, a reasonable choice for $w(\hat{t})$ is

$$w(\hat{t}) = \mathrm{e}^{\frac{-\hat{t}}{\gamma\tau}}, \tag{32}$$

where $\gamma = t_s/\tau$ is the ratio of the short delay to the long one and it will be assumed constant. This choice of an exponential term for the weight function implies that the effect of the continuous delay disappears gradually as $t_s \to \infty$, see Fig. 8. With this choice for $w(\hat{t})$, the continuous delay term in Eq. (30) can be eliminated by first differentiating the equation with respect to time to obtain

$$\ddot{x}(t) + \alpha\dot{x}(t) + \beta\int_0^\infty \dot{x}(t-\tau-\hat{t})\mathrm{e}^{\frac{-\hat{t}}{\gamma\tau}}\mathrm{d}\hat{t} = 0. \tag{33}$$

Note that differentiating the original DIDE does not produce a system that is completely equivalent to the original DIDE [29,16]. Specifically, (i) whereas the zero solution is the only steady state solution of the original DIDE, the differentiated equation is satisfied for any constant solution. Further, the stability of the zero solution of both systems is not completely equivalent since the characteristic equations of the differentiated equation will always have an additional zero root. Nevertheless, besides the extra root, all the other roots coincide with those of the original DIDE. Therefore, the stability of the original DIDE can practically be investigated by studying the stability of the differentiated equation [29,16].

Therefore, we proceed by integrating the continuous delay term by parts – utilizing the assumption in Eq. (31) – to obtain

$$\begin{aligned}\beta\int_0^\infty \dot{x}(t-\tau-\hat{t})\mathrm{e}^{\frac{-\hat{t}}{\gamma\tau}}\mathrm{d}\hat{t} &= -\beta\left[x(t-\tau-\hat{t})\,\mathrm{e}^{\frac{-\hat{t}}{\gamma\tau}}\Big|_0^\infty + \frac{1}{\gamma\tau}\int_0^\infty x(t-\tau-\hat{t})\mathrm{e}^{\frac{-\hat{t}}{\gamma\tau}}\mathrm{d}\hat{t}\right]\\ &= \beta x(t-\tau) + \frac{1}{\gamma\tau}[\dot{x}(t) + \alpha x(t)].\end{aligned} \tag{34}$$

Finally, substituting Eq. (34) into Eq. (33) gives

$$\ddot{x}(t) + \left(\alpha + \frac{1}{\gamma\tau}\right)\dot{x}(t) + \frac{\alpha}{\gamma\tau}\beta x(t-\tau) = 0, \tag{35}$$

or in state-space form

$$\begin{bmatrix}\dot{y}_1\\ \dot{y}_2\end{bmatrix} = \begin{bmatrix}0 & 1\\ \dfrac{-\alpha}{\gamma\tau} & -\left(\alpha + \dfrac{1}{\gamma\tau}\right)\end{bmatrix}\begin{bmatrix}y_1\\ y_2\end{bmatrix} + \begin{bmatrix}0 & 0\\ -\beta & 0\end{bmatrix}\begin{bmatrix}y_1(t-\tau)\\ y_2(t-\tau)\end{bmatrix}, \tag{36}$$

where now Eq. (35) represents a transformation of Eq. (30) that contains the discrete delay only. The analysis techniques for DDEs with discrete delays can then be used to investigate the stability of Eq. (35). Fig. 9 shows the stability chart for Eq. (30) for $\gamma = 0.5$ and 1.5 assuming a discrete delay $\tau = 1$.

Therefore, the methods described here successfully transformed the complicated distributed delay problem into a higher-order, simpler DDE that can be handled using the methods for discrete DDEs. Although the described transformation works only for gamma-type distribution, these types of distributions appear in a vast variety of applications including machining dynamics and wheel shimmy models [10,2].

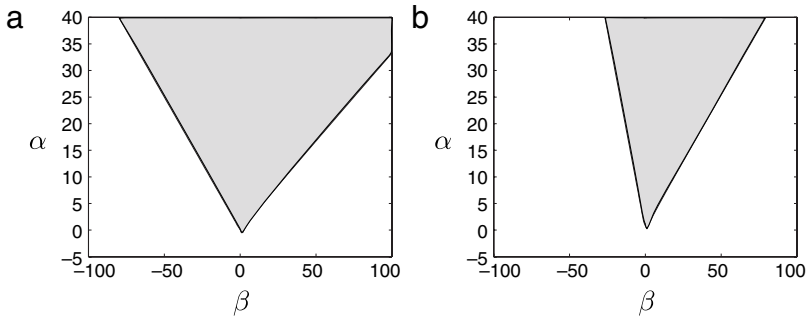

Fig. 9. Stability charts of Eq. (30) for $\tau = 1$, and (A) $\gamma = 0.5$ and (B) $\gamma = 1.5$. Moreover, a grid of 100×100 and $E = 10$ were used. Stable regions are shaded while unstable regions are left unshaded.

4. Conclusions

This paper described a spectral element approach for studying the stability of delay integro-differential equations (DIDEs). In comparison to DDEs with a discrete delay, the analysis of DIDEs is more complicated due to the integral term which maps single points onto intervals. The distributed delay term was approximated using a Legendre–Gauss–Lobatto quadrature with $m + 1$ quadrature points. This approximation caused each discretization node in the interval $[0, T]$ to map onto $m + 1$ points. The mapped points were interpolated in terms of the local discretization nodes within each element.

To demonstrate the effectiveness of the developed approach, the stability of several case studies was investigated. The first case study was a scalar DIDE with constant kernel, see Fig. 5. The second case study was a time-periodic DIDE with time-dependent kernel function. The stability diagrams for this case are shown in Figs. 6 and 7. The stability diagrams were in agreement with those obtained using well-established methods in literature, namely *D*-subdivision and the semi-discretization technique. However, it was found that due to the large number of mappings associated with the integral term, the time required to produce the stability diagrams was significantly larger than the discrete delay case.

The case of special kernel functions was investigated in Section 3. These constant or gamma-type distribution functions appear in many physical models, such as low speed milling and wheel shimmy, and they allow the DIDE to be transformed into a higher order DDE with only discrete delays. The stability of the original DIDE can then be investigated using the simpler transformed DDE.

References

[1] G. Stépán, Delay nonlinear oscillations and shimmying wheels, in: F.C. Moon (Ed.), Applications of Nonlinear and Chaotic Dynamics in Mechanics, 1st ed., Kluwer Academic Publisher, Dordrecht, 1998, pp. 373–386.
[2] D. Takács, G. Stépán, S.J. Hogan, Isolated large amplitude periodic motions of towed rigid wheels, Nonlinear Dynamics 52 (1) (2007) 27–34.
[3] D. Takács, G. Orosz, G. Stépán, Delay effects in shimmy dynamics of wheels with stretched string-like tyres, European Journal of Mechanics—A/Solids 28 (3) (2009) 516–525. doi:10.1016/j.euromechsol.2008.11.007.
[4] M. Bando, K. Hasebe, K. Nakanishi, A. Nakayama, Analysis of optimal velocity model with explicit delay, Physical Review E 58 (5) (1998) 5429–5435. doi:10.1103/PhysRevE.58.5429.
[5] G. Orosz, R. Wilson, B. Krauskopf, Global bifurcation investigation of an optimal velocity traffic model with driver reaction time, Physical Review E 70 (2) (2004) 026207. doi:10.1103/PhysRevE.70.026207.
[6] G. Orosz, G. Stépán, Subcritical hopf bifurcations in a car-following model with reaction-time delay, Proceedings of the Royal Society A 462 (2073) (2006) 2643–2670. doi:10.1098/rspa.2006.1660.
[7] R. Sipahi, F. Atay, S.-I. Niculescu, Stability of traffic flow behavior with distributed delays modeling the memory effects of the drivers, SIAM Journal of Applied Mathematics 68 (3) (2007) 738–759. doi:10.1137/060673813.
[8] W. Michiels, C.-I. Morărescu, S.-I. Niculescu, Consensus problems with distributed delays, with application to traffic flow models, SIAM Journal on Control and Optimization 48 (1) (2009) 77–101. doi:10.1137/060671425.
[9] G. Stépán, Retarded Dynamical Sytems: Stability and Characteristic Functions, John Wiley & Sons, 1989.
[10] F. Khasawneh, B. Mann, T. Insperger, G. Stépán, Increased stability of low-speed turning through a distributed force and continuous delay model, Journal of Computational and Nonlinear Dynamics 4 (4) (2009) 041003.
[11] S. Campbell, Time delays in neural systems, in: Handbook of Brain Connectivity, Springer-Verlag, 2007, pp. 65-90.
[12] T. Koto, Stability of Runge–Kutta methods for delay integro-differential equations, Journal of Computational and Applied Mathematics 145 (2) (2002) 483–492. doi:10.1016/S0377-0427(01)00596-9.
[13] C. Zhang, S. Vandewalle, Stability analysis of Runge–Kutta methods for nonlinear Volterra delay-integro-differential equations, IMA Journal of Numerical Analysis 24 (2004) 193–214. (22).
[14] C. Baker, N. Ford, Stability properties of a scheme for the approximate solution of a delay-integro-differential equation, Applied Numerical Mathematics 9 (3–5) (1992) 357–370. doi:10.1016/0168-9274(92)90027-B.
[15] T. Luzyanina, K. Engelborghs, D. Roose, Computing stability of differential equations with bounded distributed delays, Numerical Algorithms 34 (1) (2003) 41–66. doi:10.1023/A:1026194503720.
[16] T. Luzyanina, D. Roose, Equations with distributed delays: bifurcation analysis using computational tools for discrete delay equations, Functional Differential Equations 11 (1–2) (2004) 87–92.
[17] G. Kiss, B. Krauskopf, Stability implications of delay distribution for first-order and second-order systems, Discrete and Continuous Dynamical Systems-series B 13 (2) (2010) 327–345. doi:10.3934/dcdsb.2010.13.327.
[18] G. Kiss, B. Krauskopf, Stabilizing effect of delay distribution for a class of second-order systems without instantaneous feedback, Dynamical Systems: An International Journal 26 (1) (2011) 85–101. doi:10.1080/14689367.2010.523889.

[19] T. Insperger, G. Stépán, Semi-discretization method for delayed systems, International Journal for Numerical Methods in Engineering 55 (2002) 503–518.
[20] T. Insperger, G. Stépán, J. Turi, On the higher-order semi-discretizations for periodic delayed systems, Journal of Sound and Vibration 313 (2008) 334–341.
[21] D. Breda, S. Maset, R. Vermiglio, Computing the characteristic roots for delay differential equations, IMA Journal of Numerical Analysis 24 (1) (2004) 1–19. doi:10.1093/imanum/24.1.1.
[22] F.A. Khasawneh, B.P. Mann, A spectral element approach for the stability of delay systems, International Journal for Numerical Methods in Engineering (2011) doi:10.1002/nme.3122. n/a–n/a.
[23] T.H. Vu, A.J. Deeks, Use of higher-order shape functions in the scaled boundary finite element method, International Journal for Numerical Methods in Engineering 65 (2006) 1714–1733.
[24] J. Berrut, L.N. Trefethen, Barycentric Lagrange interpolation, SIAM Review 46 (3) (2004) 501–517.
[25] N. Higham, The numerical stability of Barycentric Lagrange interpolation, IMA Journal of Numerical Analysis 24 (4) (2004) 547–556. doi:10.1093/imanum/24.4.547. arXiv:http://imajna.oxfordjournals.org/cgi/reprint/24/4/547.pdf.
[26] K. Engelborghs, E. Doedel, Stability of piecewise polynomial collocation for computing periodic solutions of delay differential equations, Numerische Mathematik 91 (2002) 627–648.
[27] J.P. Boyd, Chebyshev and Fourier Spectral Methods, Dover Publications, 2001.
[28] F. Khasawneh, B. Mann, T. Insperger, G. Stépán, Explanation for low-speed stability increases in machining: application of a continuous delay model, in: Proceedings of the ASME 2008 Dynamic Systems and Control Conference, Invited Session on "Time-Delay Systems, from Theory to Applications", October 20–22, 2008, Ann Arbor, Michigan, USA, No. DSCC2008-2287, 2008.
[29] K. Cooke, W. Huang, On the problem of linearization for state-dependent delay differential equations, Proceedings of the American Mathematical Society 124 (5) (1996) 1417–1426.